Vibronic Coupling Effects in the Photoelectron Spectrum of Ozone: A Coupled-Cluster Approach

Paweł Wójcik[a], Hanna Reisler[a], Péter G. Szalay[b], Anna I. Krylov[a,†], John F. Stanton[b,c,*]

[a] Department of Chemistry, University of Southern California, Los Angeles, California 90089, USA

[b] Laboratory of Theoretical Chemistry, Institute of Chemistry, ELTE Eötvös Loránd University, Pázmány Péter stny. 1/A, Budapest, Hungary

[c] Quantum Theory Project, Departments of Chemistry and Physics, University of Florida, Gainesville, FL, USA 32611

† krylov@usc.edu; * jfstanton137@gmail.com

(Dated: October 31, 2024)

Abstract

One of the most important areas of application for equation-of-motion coupled cluster (EOM-CC) theory is the prediction, simulation, and analysis of various types of electronic spectra. In this work, the EOM-CC method for ionized states, known as EOM-IP-CC, is applied to the closely lying and coupled pair of states of the ozone cation — $\tilde{X}^2A_1$ and $\tilde{A}^2B_2$ — using highly accurate treatments including up to the full single, double, triple, and quadruple excitations (EOM-IP-CCSDTQ). Combined with a venerable and powerful method for calculating vibronic spectra from the Hamiltonian produced by EOM-IP-CC calculations, the simulations yield a spectrum that is in good agreement with the photoelectron spectrum of ozone. Importantly, the calculations suggest that the adiabatic gap separating these two electronic states is somewhat smaller than currently thought; an assignment of the simulated spectrum together with the more precise band positions of the experimental measurements suggests T_{00}=1,368±65 cm^{-1}.

I. INTRODUCTION

Amongst the brotherhood of triatomic molecules, it cannot be denied that water (H_2O) is the most important, the most highly studied, and the most well-understood. Beyond H_2O, many triatomic molecules that have an environmental, technological or biological impor-

tance have been subjected to many studies and are understood to various levels of detail. Perhaps the most interesting such case is ozone (O_3), which has a vast number of important properties, a very rich history of study[1], and unlike the relatively simple water molecule, a profound quantum-mechanical complexity[2]. Structurally, while we think of ozone as having two distinct kinds of oxygen atoms (and an NMR experiment would reveal that), the full molecular Hamiltonian does not distinguish between them. Rather, it yields the three equivalent structures separated by a barrier that lies tantalizingly close to the $O_3 \rightarrow O_2 + O$ dissociation threshold (102.4 kJ/mol)[3], as shown in Fig. 1. In reality, the energy levels of ozone all have a near triple $(e + a)$ degeneracy, albeit with a tunneling splitting so small that it can be ignored, along with a semi-infinite lifetime (despite opposing opinion[4]). More than a half century ago, this intriguing aspect of the ozone molecule was first discussed by Berry[5].

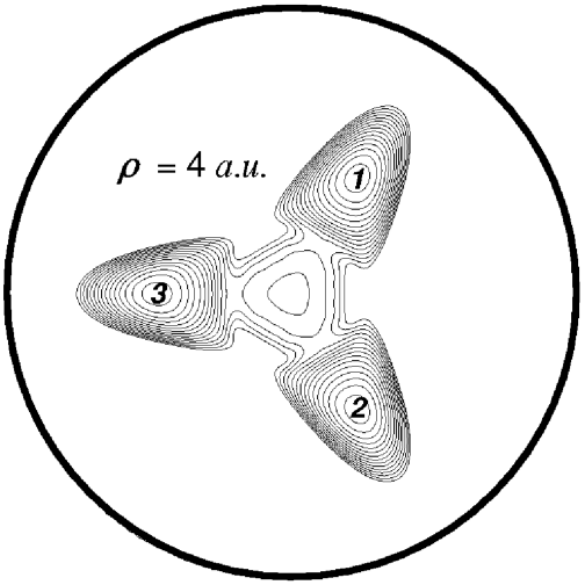

FIG. 1: Two-dimensional slice of the potential energy surface of ozone in hyperspherical coordinates at the value of hyperradiuns ρ=4 a.u. (the lowest contour is at 1 eV below the dissociation limit). The slice shows three equivalent minima corresponding to C_{2v} structures separated by large barriers. Reproduced with permission from Ref. 6. Copyright 2003 American Institute of Physics.

Beyond the structural aspects of ozone, other mysteries surround this curious molecule. For example, the distribution of the eighteen distinct $^{16}O/^{17}O/^{18}O$ isotopologues in the Earth's atmosphere differs from what is expected based on the natural isotopic abundance,

a puzzle that has been open for more than three decades[6,7].

Among quantum chemists, ozone has a notorious history, owing to its strong diradical character causing significant difficulties in calculations of its ostensibly simple ground-state molecular properties. An early 1989 study[8,9] by the Bartlett group and collaborators found that the CCSD+T(CCSD) method predicted that the molecular equilibrium structure of ozone would have C_s symmetry (that is, the asymmetric stretching harmonic frequency computed by this method is imaginary), a finding that led to a search for better treatment of non-iterative triple excitations, ultimately leading to the well-known CCSD(T) method[10–12]. While CCSD(T) and higher-level coupled-cluster methods available today[13–15] do a good job in describing the equilibrium structure and vibrational potential, an elaborate multireference configuration interaction calculations can describe the entire ground-state surface out to the dissociation limit[6,16,17], facilitating calculations of spectroscopy and chemical reactions of ozone. As such, the quantum chemical understanding and fidelity for the ground electronic state of O_3 is now at a mature level.

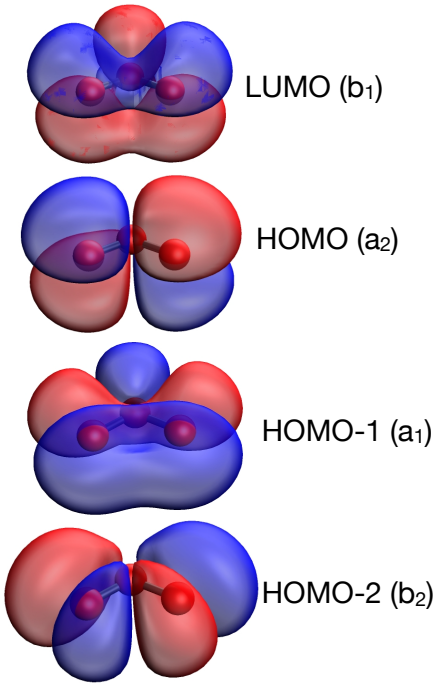

FIG. 2: Frontier molecular orbitals of ozone; HF/6-31G*. The lowest states of the ozone cation are $^2A_1$ and $^2B_2$ derived by ionization from the HOMO-1 and HOMO-2, respectively.

Qualitatively, the challenge posed to electronic structure theory by ozone ultimately arises from its closely spaced highest-occupied (a_2) and lowest-unoccupied (b_1) molecular orbitals

(HOMO and LUMO, respectively; see Fig. 2), giving rise to the following wavefunction:

$$X^1A_1 = C_1[core]^6(3a_1)^2(2b_2)^2(4a_1)^2(5a_1)^2(3b_2)^2(1b_1)^2(4b_2)^2(6a_1)^2(1a_2)^2(2b_1)^0 + \quad (1)$$

$$C_2[core]^6(3a_1)^2(2b_2)^2(4a_1)^2(5a_1)^2(3b_2)^2(1b_1)^2(4b_2)^2(6a_1)^2(1a_2)^0(2b_1)^2. \quad (2)$$

The two electron configurations $[\cdots]a_2^2b_1^0$ and $[\cdots]a_2^0b_1^2$ mix strongly (the coefficients of these two leading configurations are C_1 ≈0.9 and C_2 ≈0.3, according to the EOM-SF-CCSD (EOM-CCSD with spin-flip) calculations[18]), posing the aforementioned challenges with (especially single-reference) quantum-chemical methods. A second feature consequence of the symmetry and energetic proximity of these two orbitals is that the ozone cation (which is isoelectronic to the NO_2 radical) has closely lying $^2A_1$ and $^2B_2$ electronic states derived by ionization from the HOMO-1 and HOMO-2, respectively (see Fig. 2). Like the associated states in NO_2, these two states are plagued by orbital symmetry breaking[19], a problem that greatly complicates their quantum-chemical treatment. One of the many accomplishments of the Bartlett group has been their integral role in the development of equation-of-motion coupled-cluster theory[20–22] (EOM-CC, also known as linear response coupled-cluster theory[23]). These methods provide a very efficient and simple way to treat certain classes of electronic structure that are often termed "multireference problems"[24,25], and are ideally suited to studying reactive intermediates, radicals, diradicals, and electronically excited states. From a somewhat wider viewpoint, the existence of closely spaced electronic states always carries the potential for (possibly strong) vibronic coupling, a phenomenon that can play an important role in molecular dynamics and spectroscopy. Indeed, one of the great successes of EOM-CC methods has been in their ability — if and only if combined with vibronic coupling models — to enable high-quality simulations of complicated electronic spectra. Such work provides important insights into the nature of vibronic coupling in molecular systems, as has been exemplified by various application studies (for example, see Refs. 26 and 27). In the case of ozone cation, the two lowest electronic states separated by a small gap of ∼0.1 eV are coupled by the asymmetric stretch of b_2 symmetry (Fig. 3).

The photoelectron spectrum of ozone was reported[28] in 1974. Later, much higher resolution of the positions of vibronic peaks was obtained with pulsed-field-ionization zero-kinetic-energy (PFI-ZEKE) spectroscopy[29]. From the theory side, the vibronic photoelectron spectrum of ozone was modeled with a vibronic Hamiltonian parameterized using multi-reference configuration interaction method by Tarroni and Carter[29].

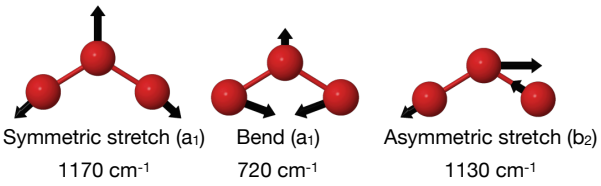

FIG. 3: Three normal modes of the neutral ozone CCSDT/ANO1. Asymmetric stretching vibration of b_2 symmetry can couple the two lowest states of the cation ($^2A_1$ and $^2B_2$).

Our contribution to this issue paying homage to the career and accomplishments of R.J. Bartlett consists of an application of a vibronic coupling model, parametrized by EOM-CC calculations, to the photoelectron spectrum of ozone. We trust that this combination of methodology applied to a molecule that has been extensively studied by the Bartlett group is an appropriate contribution.

II. THEORETICAL MODELS AND COMPUTATIONAL DETAILS

Ozone is a C_{2v} molecule (following Mulliken's convention[30], the molecule is placed in the yz-plane and the molecular symmetry axis aligns with the z-direction) with three normal modes: symmetric stretch, symmetric bend, and asymmetric stretch (Fig. 3). The asymmetric stretch is of b_2 symmetry. The two lowest electronic states of the ozone cation, $^2A_1$ and $^2B_2$, are very close in energy—separated by the vertical gap (at the neutral's geometry) of mere 0.123 eV (or 990 cm^{-1}, see Table 2)—and can be coupled by the b_2 vibration, giving rise to significant vibronic effects in the photoelectron spectrum. The vertical gap corresponds to the difference in the energies of electronic states at the same geometry (here, the structure of the neutral). While vertical energy gap is easy to compute, they are not observable experimentally. The experimentally accessible value is the adiabatic gap T_{00}—the energy difference between the vibronic levels of the two state.

We simulate the vibronic states of the ozone cation using the model Hamiltonian of Köppel, Domcke, and Cederbaum—the KDC Hamiltonian[31–33]. This is a multi-state and multi-mode Hamiltonian defined in the basis of diabatic states. For the ozone cation, the basis comprises two quasi-diabatic states (related to the $^2A_1$ and $^2B_2$ states at the minimum of neutral ozone), coupled by one mode (asymmetric stretch, mode number 3). The model also includes two symmetric modes (modes number 1 and 2). The matrix elements of

the vibronic Hamiltonian are expanded around the equilibrium geometry of neutral ozone using the respective dimensionless normal coordinates, Q_i, and the corresponding harmonic frequencies, ω_i. The overall form of the vibronic Hamiltonian is thus:

$$H = H_0\mathbf{1} + \begin{pmatrix} V^{(1)} & \lambda_3 Q_3 \\ \lambda_3 Q_3 & V^{(2)} \end{pmatrix}, \tag{3a}$$

where H_0 contains kinetic energy operator and a potential energy term for the coupling mode

$$H_0 = \frac{1}{2}\left(\sum_{i=1}^{3} -\omega_i \frac{\partial^2}{\partial Q_i^2}\right) + \frac{1}{2}\omega_3 Q_3^2, \tag{3b}$$

and $V^{(1)}$ and $V^{(2)}$ describe the two diabatic states expanded over Q_1 and Q_2

$$V^{(\alpha)} = E^{(\alpha)} + \sum_{i\in\{1,2\}} \kappa_i^{(\alpha)} Q_i + \sum_{i,j\in\{1,2\}} \kappa_{ij}^{(\alpha)} Q_i Q_j + \sum_{i,j,k\in\{1,2\}} \kappa_{ijk}^{(\alpha)} Q_i Q_j Q_k + \sum_{i,j,k,l\in\{1,2\}} \kappa_{ijkl}^{(\alpha)} Q_i Q_j Q_k Q_l. \tag{3c}$$

Here $E^{(\alpha)}$ are the vertical ionization energies calculated at the equilibrium geometry of the neutral, κ are the coefficients of expansion of the potential along the fully symmetric coordinates, and λ is the linear diabatic coupling. Fig. 4 shows the resulting diabatic potential energy surfaces (the corresponding contour plots are shown in the SI). The displacements along the two symmetric normal modes are clearly visible, suggesting vibrational progressions along the bend and symmetric stretch.

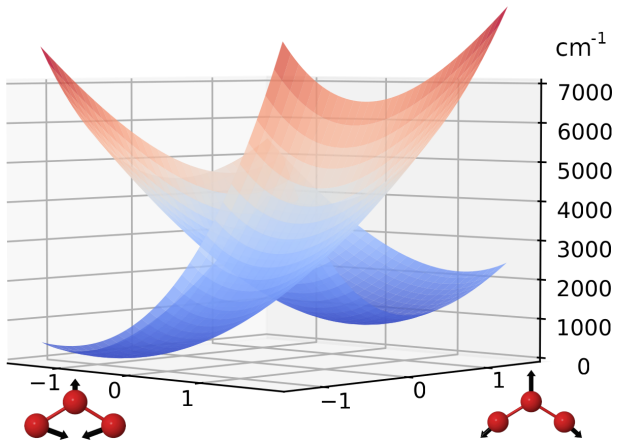

FIG. 4: Cuts of potential energy surfaces of the two diabatic states of the ozone cation (corresponding to the $^2A_1$ and $^2B_2$ states at the equilibrium geometry of the neutral) shown as function of the two symmetric modes in dimensionless normal coordinates, Q_1 and Q_2, at Q_3=0.

We computed the parameters of the KDC Hamiltonian using *ab initio* CC and EOM-CC methods.[22,24,25,34–36] We considered methods in which the CC expansion was truncated to singles and doubles (CCSD), singles, doubles and triples (CCSDT), as well as singles, doubles, triples, and quadruples (CCSDTQ).[15] We computed the geometry of the neutral ozone and its harmonic frequencies and normal coordinates with CCSDT/ANO1[37,38]; the Cartesian coordinates are given in the SI.

At the optimized geometry, ozone has a bond length of 1.270 Å and a bond angle of 116.9°. The two symmetric normal modes have frequencies 1,170 cm^{-1} and 720 cm^{-1}, and the asymmetric stretch has a frequency of 1,130 cm^{-1}.

We described the states of the cation using EOM-CC for ionization energies (known as EOM-IP-CC).[39] We used the definition of quasi-diabatic states by Ichino, Gauss, and Stanton[40] based on the EOM-IP-CC method (EOMIP-CC-QD). We computed the linear diabatic coupling λ and the expansion coefficients κ at the equilibrium geometry of the neutral; λ was computed with EOM-IP-CCSD-QD/ANO1. A grid of 17x17 points stretching from -0.2 to 0.2 units along the dimensionless normal coordinates of the symmetric modes was used to calculate the EOM-IP-CCSD/ANO1 energies that were fitted into the 4th order polynomial in these coordinate to extract the κ parameters. The computed value of the linear diabatic coupling constant λ is 1,394 cm^{-1}. The complete set of KDC parameters is given in the SI.

We computed the vertical ionization energies at the geometry of the neutral ozone using a composite method. The starting value is the complete basis set (CBS) extrapolation of the EOM-IP-CCSDT/cc-pCVnZ energies with n = 5, 6.[41] These values were augmented with two corrections: the ΔQ (quadrupoles) correction in the cc-pwCVTZ basis set and the relativistic correction calculated using EOM-IP-CCSD/cc-pwCVTZ.[42] The error bars were estimated as follows: for the extrapolated CBS reference values, we used half of the absolute value of the difference between the best *ab initio* value and the extrapolated value, and for the remaining corrections (quadruples correction, ΔQ, and the relativistic correction) we used half of the absolute value of the correction.

To compare the simulated photoelectron spectrum to the experimental one, we used the cross-section ratio A_1:B_2 of 1:1.35.[43] Additionally, the stick spectrum was broadened with

the Lorenzian envelopes normalized to the feature intensities

$$f(x, x_i, I_i) = \frac{I_i}{(x - x_i)^2 + (\gamma/2)^2}, \tag{4}$$

where x_i is the position of the spectral peak, I_i is its intensity and γ is the peak's width.

The spectrum was computed using the XSIM module in CFOUR, with the basis of 50 harmonic states in each mode and 6,000 iterations of the Lanczos procedure, starting from the seed vector with no vibrational excitations, i.e, $|\text{seed}\rangle = |0 \ldots 0\rangle$.[44] All electrons were correlated in all CC/EOM-CC calculations. All calculations were performed using CFOUR.[45,46]

III. RESULTS AND DISCUSSION

We begin by discussing the accuracy of the computed electronic states. The vertical ionization energy for the first excited state, $E^{(1)}$, computed using the composite method described above, is 12.827 eV. Our error estimate for this value is 30 meV (see Table 1 for details). We note that the convergence of the vertical gap between the two states is much faster and this value is estimated as 123±8 meV (see Table 2 for details).

TABLE 1: Vertical ionization energies with the error estimates, eV.

Contribution	$^2A_1$	$^2B_2$	Error estimate
EOM-CCSDT/CBS	12.872	12.981	0.02
ΔQ/pwCVTZ	-0.037	-0.021	0.02
Relativistic/CCSD/pwCVTZ	-0.008	-0.010	0.005
Final value, eV	12.827	12.950	0.03

Figure 5 compares the simulated spectrum to the lower-resolution experimental spectrum taken from Ref. 28. Peak A is known to be a hot band, and does not appear in our (0 K) simulation.[43] The simulation reproduces well the consecutive increase in the intensities of peaks B, C, D, and E as well as the spacing between these peaks. The drop in the intensity at peak F is captured by the simulation. Starting from peak G, the simulation shows discrepancy with the experiment. A sudden drop in the intensity past peak H is not observed in the simulation. We discuss a likely source of this mismatch below.

TABLE 2: The vertical energy gap between the $^2A_1$ and $^2B_2$ states with error estimates, meV.

Contribution	Vertical gap	Error estimate
EOM-CCSDT/CBS	108.8	0.9
ΔQ/pwCVTZ	16.5	8
Relativistic/CCSD/pwCVTZ	-2.2	1.1
Final value, meV	123	8
Final value, cm^{-1}	990	65

Our simulation allows for an additional element of analysis—Figure 6 shows a decomposition of the simulated spectrum from Figure 5. All lines that contribute to the spectrum are marked individually and are color-coded indicating which electronic state's transition intensity the peak draws from. The total envelope of the spectrum is also decomposed showing contributions from each state. Our simulation locates the minimum of the conical intersection (marked as CI) at 3,174 cm^{-1} above the origin (12.92 eV), where origin means the lowest energy peak appearing in the spectrum. The adiabatic energy gap between the two lowest vibrational states in each of the cation states is T_{00}=1,368±65 cm^{-1}.

We assigned the vibronic peaks by comparing to the Franck–Condon simulation. To this end, the spectrum is simulated once again, this time, however, setting the linear diabatic constant to zero (λ= 0). This yields the spectra of the two electronic states at an equivalent level of theory but without vibronic coupling, i.e., the combined Franck–Condon spectra of the two states. Figure 7 shows this spectrum. The non-coupled spectrum is easy to assign using the labels that mark the symmetry of the electronic state, A_1 or B_2, and the vibrational state ($\nu_1\nu_2\nu_3$), where ν_i is the number of quanta in mode i ($i = 1$ for the symmetric stretch, $i = 2$ for the symmetric bend and $i = 3$ for the asymmetric stretch). The assigned spectrum shows progressions in the symmetric bend. There is one such progression in each electronic state. Additionally for each state, there is also another progression in the symmetric bend with one excitation in the symmetric stretch.

The decomposition of the spectrum presented on Figure 6 provides additional insight. The spectrum shows that peaks B and C are almost purely of the $^2A_1$ electronic and a_1 vibrational character. Starting from peak D, the contributions from two states are of equal magnitude.

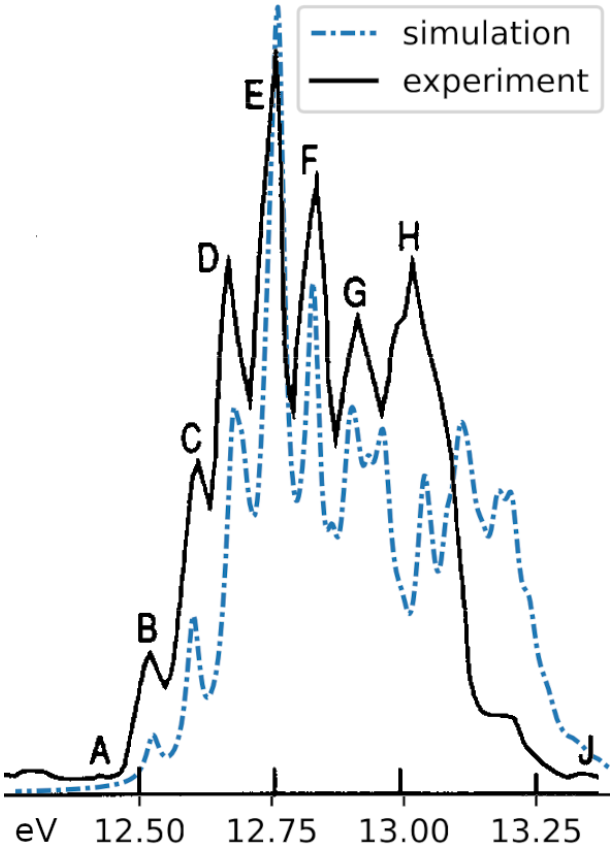

FIG. 5: Comparison of the experimental (solid black line digitized from Ref. 28) and the simulated photoelectron spectra shown as electron binding energies. The simulated spectrum is blue-shifted by 21 meV and the peaks were broadened using $\gamma = 30$ meV. Reproduced with permission from Ref. 28. Copyright 1974 Royal Society of Chemistry.

It is also clear that the following peaks are mixtures of many vibronic peaks. At the energy of about 2,000 cm^{-1} above the origin the density of vibronic peaks increases significantly. This value can be compared to the minimum of the conical intersection located at about 1000 cm^{-1} higher in energy, at 3,174 cm^{-1} above the origin. Our Hamiltonian is not suitable for describing the dissociation of the molecule, therefore, we expect a discrepancy with the experiment as the energy gets closer to the dissociation threshold located at 4,898±3 cm^{-1} above the origin.[29]

Figure 8 shows the assigned spectrum and Table 3 lists the decomposition of all peaks in the region of up to 3100 cm^{-1}. We compare the resulting assignment with the high-resolution PFI-ZEKE spectrum from Ref. 29. The PFI-ZEKE spectrum is the best source of information on the location of the peaks, especially the origin, against which the origin

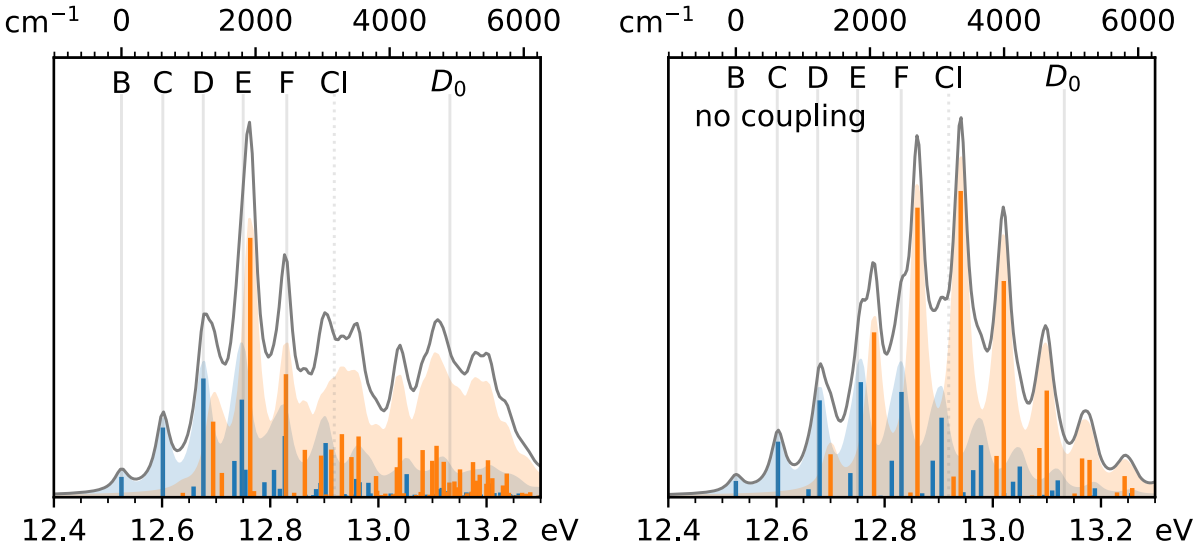

FIG. 6: Simulated photoelectron spectrum of ozone shown as electron binding energies. Bottom axis shows energy scale in eV. Top axis shows energy offset from the origin in cm^{-1}. Stick spectrum shows positions and intensities of all simulated states. Blue and orange colors mark states of A_1 and B_2 symmetry, respectively. Gray vertical lines with captions on top indicate positions of features measured by the PFI-ZEKE experiment.[29] The simulated spectrum was shifted to match the PFI-ZEKE experimental origin by 21 meV. D_0 marks the dissociation threshold of O_3^+.[29] Gray dotted line marks the energy of the minimum of the conical intersection (CI) as located by our Hamiltonian. The right panel shows the uncoupled spectrum (the same as in Fig. 7 but formatted in a matching manner).

peak of the simulation is aligned. The origin of the simulated spectrum is red-shifted by 170 cm^{-1} relative to the experimental origin at 101,020.5 cm^{-1}.[29] This discrepancy is within our error estimate for the vertical ionization energy (30 meV=240 cm^{-1}).

The comparison with the high-resolution spectrum (Fig. 8) reveals more details. Lines of the PFI-ZEKE experiment and our simulation match very well. Especially the states of A_1 symmetry are well aligned with the experimental features. States close to the origin are similar to the non-coupled states. The origin peak is of $A_1(0,0,0)$ character, the first two excitations in the symmetric bend, $A_1(0,1,0)$ and $A_1(0,2,0)$ are also very similar to the non-coupled states, whereas the higher excitations in this progression show significant mixing. The same progression with one vibrational quanta in the symmetric stretch is more

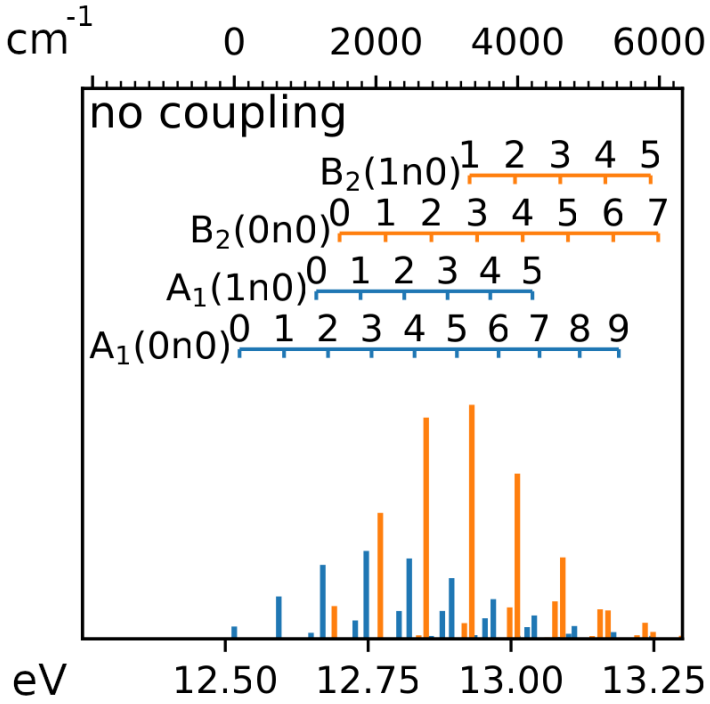

FIG. 7: Simulated Franck–Condon photoelectron spectrum of ozone with vibronic coupling removed.

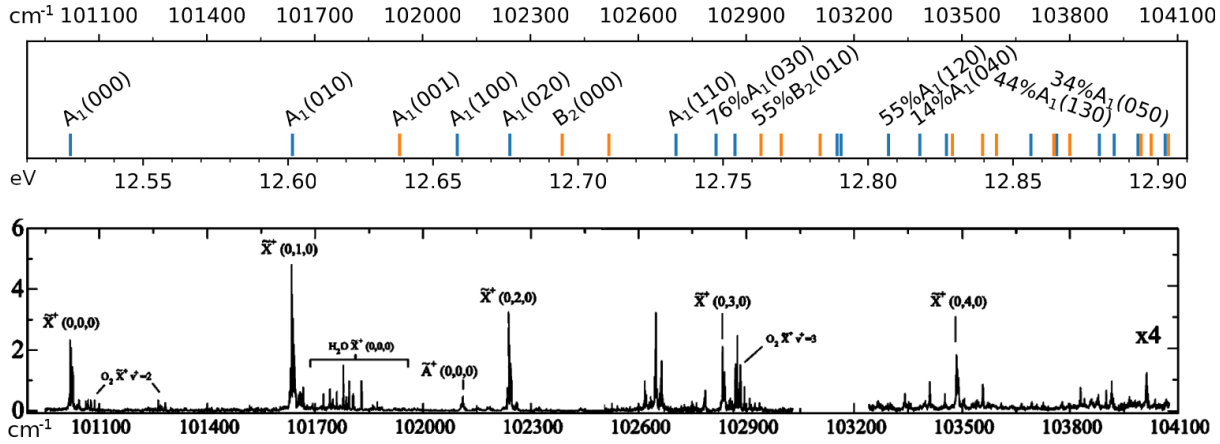

FIG. 8: Comparison of the simulated spectrum with the PFI-ZEKE experiment.[29] The simulated spectrum was blue-shifted by 21 meV = 170 cm^{-1}. Color of the simulated peaks marks the symmetry of the vibronic states: A_1 are colored blue and B_2 are colored orange. See Table 3 for a detailed listing of state assignments. The bottom panel reproduced with permission from Ref. 29. Copyright 2005 American Institute of Physics.

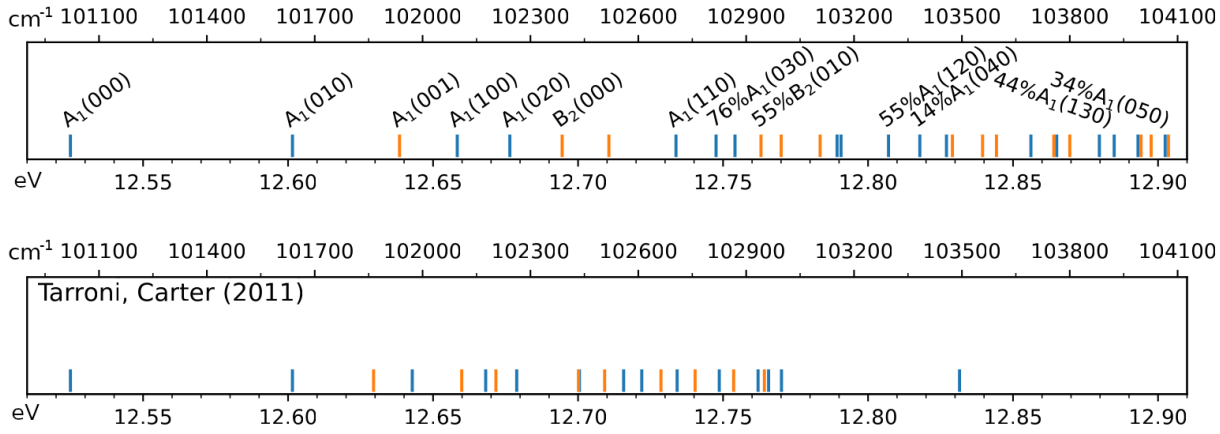

FIG. 9: Comparison of the simulated spectrum to an earlier simulation by Tarroni and Carter (assigned lines).[47]

interesting. The first of its peaks is very well aligned with experimentally visible feature, which was previously assigned as the origin of the second electronic state. The second peak in this series, $A_1(1,1,0)$, has very high similarity to its uncoupled version. It is a good candidate to assign the experimental, unassigned feature above 102,600 cm^{-1}.

States of B_2 symmetry, on the other hand, do not align well with the experiment. The first such peak, close to the 12.64 eV mark in Figure 8, is assigned to the $A_1(0,0,1)$ state. This is a vibronic state that gains intensity owing to the coupling to the electronic $^2B_2$ state. This vibronic peak lies in the part of the spectrum where bands of oxygen (which is an impurity in the gas sample) are visible in the experiment. The origin of the $^2B_2$ state is very similar to the uncoupled $B_2(0,0,0)$ state, but it is located in an empty area of the experimental spectrum. We use the difference in the energy between this peak and the origin peak to report the adiabatic energy gap between the two cationic states, which, according to our simulation, is T_{00}=1,368 cm^{-1}. This value is reported with an error estimate equal to the error estimate for the vertical excitation energy gap (65 cm^{-1}), which is listed Table 2. The next peak, slightly above a 12.76 eV mark in Figure 8, corresponds to one excitation of the symmetric bend in the $^2B_2$ state, but as the label on the figure shows, it is only about 55% similar to the uncoupled state.

Finally, Figure 9 compares our spectrum to an earlier accurate simulation by Tarroni and Carter[47]. This earlier work used internally contracted multi reference configuration interaction method in a large basis set (cc-pV5Z) to thoroughly scan the vicinity of the

minima on both potentials. Similarly to our work, Tarroni and Carter did not account for the potential at distances reaching the dissociation limit. In their work, Tarroni and Carter used a diabatization method based on the adiabatic energies and configuration interaction coefficients, which avoids calculation of the non adiabatic couplings.

Figure 9 includes only the lines from the earlier simulation that were tabulated with an assignment in the article.[47] The comparison shows that both match well with the experiment. Both simulations also agree in the assignment of the first progression in the bending mode. The previous simulation, however, shows smaller spacing between the remaining lines, yielding much higher congestion of the spectrum. Additionally, the origin of the second state falls at lower energy (as compared to our simulation), which makes it align well with the peak that was assigned in the PFI-ZEKE experiment also as the origin of the second state. While an additional simulation of the line intensities would allow for the most complete comparison to the experimental spectrum, the strong alignment of the simulated peaks of A_1 symmetry with the experimental features leads us to believe that our simulation offers the best assignment of the photoelectron spectrum of ozone to date.

IV. CONCLUSION

In this exploration of the photoelectron spectrum of the ozone molecule, we have deployed cutting-edge high-order CC models together with a vibronic Hamiltonian approach to spectroscopy beyond the Born–Oppenheimer approximation[31–33]. We parameterized the Hamiltonian using EOM-IP-CC calculations and the formalism of quasi-diabatic states of Ichino, Gauss and Stanton.[40] The results of the simulation are in excellent agreement with the experimental spectrum from the ionization onset to about 2,500 cm^{-1} higher (the restriction arising from the local parametrization of the Hamiltonian). Analysis of the spectrum and its simulation underscore the importance of vibronic coupling effects in the ozone cation. Results of this work offer a state-of-the-art insight into the details of the spectrum and allows for an assignment of the experimental results. Simulated peaks that gain intensity from the $\tilde{A}B_2$ state are absent in the PFI-ZEKE spectrum, which offers an interesting avenue for further investigations.

Supplemental Information

Parameters of the KDC Hamiltonian; relevant Cartesian coordinates; additional PES plots.

V. ACKNOWLEDGMENTS

This project was initiated when three of the authors (P.W, P.G.S., and J.F.S) were in Budapest, where J.F.S. was serving as a recipient of the John von Neumann Award in STEM bestowed by the Fulbright Foundation. P.G.S. acknowledges support by National Research, Development and Innovation Fund (NKFIF) of Hungary (Grant No. 142634).

Research at USC was supported by the NSF Center for Chemical Innovation Phase I (grant no. CHE-2221453) and the U.S. Department of Energy, Basic Energy Sciences (grant no. DE-FG02-05ER15629 to H.R.). The authors wish Prof. Bartlett a happy ninth decade of life and hope that he continues to stimulate others in the field with his creative insights.

Conflicts of interest

The authors declare the following competing financial interest(s): A.I.K. is the president and a part-owner of Q-Chem, Inc.

Data availability

The data that support the findings of this study are available within the article and the associated SI.

TABLE 3: Assignment and decomposition of the eigenvectors of the ozone cation. The first column shows the offset of simulated peaks from the origin in cm^{-1}. Note that the decomposition uses the basis of uncoupled states visible in Fig. 7, as such the eigenvector decomposition does not list components along vibronic states of a mixed symmetry, e.g., $A_1(001)$ which might, artificially, appear as a lack of mixing.

Offset	Symmetry	Assignment	Eigenvector
0	A_1	$A_1(000)$	$+0.99\ A_1(000)$
618	A_1	$A_1(010)$	$+0.99\ A_1(010)$
915	B_2	$A_1(001)$	
1076	A_1	$A_1(100)$	$-0.99\ A_1(100)$
1222	A_1	$A_1(020)$	$+0.97\ A_1(020)$
1368	B_2	$B_2(000)$	$+0.97\ B_2(000)$
1498	B_2		$+0.10\ B_2(000)$
1684	A_1	$A_1(110)$	$+0.96\ A_1(110)$
1796	A_1	$A_1(030)$	$+0.87\ A_1(030) + 0.16\ A_1(110) + 0.13\ A_1(020) - 0.13\ A_1(040)$
1848	A_1		$-0.31\ A_1(030)$
1921	B_2	$B_2(010)$	$+0.74\ B_2(010) - 0.18\ B_2(020) - 0.11\ B_2(000)$
1977	B_2		$-0.24\ B_2(010)$
2085	B_2		$+0.52\ B_2(010)$
2132	A_1		$-0.25\ A_1(030) - 0.25\ A_1(040) - 0.13\ A_1(120) + 0.13\ A_1(050)$
2143	A_1		
2275	A_1	$A_1(120)$	$+0.86\ A_1(120) + 0.12\ A_1(040)$
2362	A_1		$-0.62\ A_1(040) + 0.40\ A_1(120) - 0.17\ A_1(030) + 0.11\ A_1(050)$
2437	A_1		$-0.48\ A_1(040) - 0.11\ A_1(120)$
2453	B_2	$B_2(020)$	$+0.54\ B_2(020) + 0.25\ B_2(010) - 0.17\ B_2(030)$
2537	B_2		
2576	B_2		$+0.27\ B_2(020)$
2671	A_1		$-0.48\ A_1(040) - 0.26\ A_1(050) - 0.19\ A_1(130) - 0.14\ A_1(060)$
2735	B_2		$+0.62\ B_2(020)$
2743	A_1		
2780	B_2		$+0.22\ B_2(020)$
2862	A_1	$A_1(130)$	$+0.74\ A_1(130) + 0.13\ A_1(120) - 0.13\ A_1(050)$
2903	A_1		$-0.42\ A_1(130)$
2969	A_1		$-0.25\ A_1(130) + 0.17\ A_1(050) + 0.12\ A_1(040)$
2978	B_2		$-0.24\ B_2(110) - 0.19\ B_2(020) + 0.12\ B_2(010)$
3006	B_2		$-0.20\ B_2(030) + 0.17\ B_2(110) - 0.15\ B_2(020)$
3045	A_1	$A_1(050)$	$+0.79\ A_1(050)$
3054	B_2		$+0.29\ B_2(110) - 0.25\ B_2(030) - 0.13\ B_2(020)$

References

[1] J. Chappuis, Ann. d. l'ecole Norm. Sup. **11**, 159 (1882).

[2] D. Babikov, B. K. Kendrick, R. B. Walker, R. Schinke, and R. T. Pack, Quantum origin of an anomalous isotope effect in ozone formation, Chem. Phys. Lett. **372**, 686 (2003).

[3] B. Ruscic and D. H. Bross, Active Thermochemical Tables (ATcT) Thermochemical Values ver. 1.130, 2023.

[4] P. Garcia-Fernandez, I. B. Bersuker, and J. E. Boggs, Lost topological (berry) phase factor in electronic structure calculations. example: The ozone molecule, Phys. Rev. Lett. **96**, 163005 (2006).

[5] R. S. Berry, Time-dependent measurements and molecular structure: Ozone, Rev. Mod. Phys. **32**, 447 (1960).

[6] D. Babikov, B. K. Kendrick, R. B. Walker, R. T. Pack, P. Fleurat-Lesard, and R. Schinke, Metastable states of ozone calculated on an accurate potential energy surface, J. Chem. Phys. **118**, 6298 (2003).

[7] B. Schueler, J. Morton, and K. Mauersberger, Measurement of isotopic abundances in collected stratospheric ozone samples, Geophys. Res. Lett. **17**, 1295 (1990).

[8] J. F. Stanton, W. N. Lipscomb, D. H. Magers, and R. J. Bartlett, Highly correlated single-reference studies of the o3 potential surface. i. effects of high order excitations on the equilibrium structure and harmonic force field of ozone, J. Chem. Phys. **90**, 1077 (1989).

[9] D. H. Magers, W. N. Lipscomb, R. J. Bartlett, and J. F. Stanton, The equilibrium structure and harmonic vibrational frequencies of ozone: Coupled cluster results including triple excitations, J. Chem. Phys. **91**, 1945 (1989).

[10] K. Raghavachari, G.W . Trucks, J. A. Pople, and M. Head-Gordon, A fifth-order perturbation comparison of electron correlation theories, Chem. Phys. Lett. **157**, 479 (1989).

[11] M. Urban, J. Noga, S. J. Cole, and R. J. Bartlett, Towards a full ccsdt model for electron correlation, J. Chem. Phys. **83**, 4041 (1985).

[12] J. D. Watts, J. Gauss, and R. J. Bartlett, Coupled-cluster methods with noniterative triple excitations for restricted open-shell Hartree-Fock and other general single determinant reference

functions. Energies and analytical gradients, J. Chem. Phys. **98**, 8718 (1993).

[13] S. A. Kucharski and R. J. Bartlett, The coupled-cluster single, double, triple, and quadruple excitation method, J. Chem. Phys. **97**, 4282 (1992).

[14] M. Kállay and P. R. Surján, Higher excitations in coupled-cluster theory, J. Chem. Phys. **115**, 2945 (2001).

[15] D. A. Matthews and J. F. Stanton, Non-orthogonal spin-adaptation of coupled cluster methods: A new implementation of methods including quadruple excitations, J. Chem. Phys. **142**, 064108 (2015).

[16] R. Siebert, R. Schinke, and M. Bittererová, Spectroscopy of ozone at the dissociation threshold: Quantum calculations of bound and resonance states on a new global potential energy surface, Phys. Chem. Chem. Phys. **3**, 1795 (2001).

[17] R. Dawes, P. Lolur, A. Li, B. Jiang, and H. Guo, Communication: An accurate global potential energy surface for the ground electronic state of ozone, J. Chem. Phys. **139**, 201103 (2013).

[18] S. V. Levchenko and A. I. Krylov, Equation-of-motion spin-flip coupled-cluster model with single and double substitutions: Theory and application to cyclobutadiene, J. Chem. Phys. **120**, 175 (2004).

[19] C. F. Jackels and E. R. Davidson, The two lowest energy $^2A'$ states of NO_2, J. Chem. Phys. **64**, 2908 (1976).

[20] J. F. Stanton and R. J. Bartlett, The equation of motion coupled-cluster method. A systematic biorthogonal approach to molecular excitation energies, transition probabilities, and excited state properties, J. Chem. Phys. **98**, 7029 (1993).

[21] M. Nooijen and R. J. Bartlett, Equation of motion coupled cluster method for electron attachment, J. Chem. Phys. **102**, 3629 (1995).

[22] R.J. Bartlett and M. Musiał, Coupled-cluster theory in quantum mechanics, Rev. Mod. Phys. **79**, 291 (2007).

[23] H. Koch and P. Jørgensen, Coupled cluster response functions, J. Chem. Phys. **93**, 3333 (1990).

[24] A. I. Krylov, Equation-of-motion coupled-cluster methods for open-shell and electronically excited species: The hitchhiker's guide to Fock space, Annu. Rev. Phys. Chem. **59**, 433 (2008).

[25] A. I. Krylov, The quantum chemistry of open-shell species, in *Reviews in Comp. Chem.*, edited by A. L. Parrill and K. B. Lipkowitz, volume 30, pages 151–224. J. Wiley & Sons, 2017.

[26] J. F. Stanton, On the vibronic level structure in the NO_3 radical. I. The ground electronic state,

J. Chem. Phys. **126**, 134309 (2007).

[27] H. Köppel, M. Döscher, I. Baldea, H.-D. Meyer, and P. G. Szalay, Multistate vibronic interactions in the benzene radical cation. II. Quantum dynamical simulations, J. Chem. Phys. **117**, 2657 (2002).

[28] J. M. Dyke, L. Golob, N. Jonathan, A. Morris, and M. Okuda, Vacuum ultraviolet photoelectron spectroscopy of transient species. Part 4.–Difluoromethylene and ozone, J. Chem. Soc., Faraday Trans. 2 **70**, 1828 (1974).

[29] S. Willitsch, F. Innocenti, J. M. Dyke, and F. Merkt, High-resolution pulsed-field-ionization zero-kinetic-energy photoelectron spectroscopic study of the two lowest electronic states of the ozone cation O_3^+, J. Chem. Phys. **122**, 024311 (2005).

[30] R. S. Mulliken, Report on notation for the spectra of polyatomic molecules, J. Chem. Phys. **23**, 1997 (1955).

[31] H. Köppel, W. Domcke, and L.S. Cederbaum, Multimode molecular dynamics beyond the Born–Oppenheimer approximation, Adv. Chem. Phys. **57**, 59 (1984).

[32] W. Domcke, H. Köppel, and L. S. Cederbaum, Spectroscopic effects of conical intersections of molecular potential energy surfaces, Mol. Phys. **43**, 851 (1981).

[33] H. Köppel, W. Domcke, and L. S. Cederbaum, *The multi-mode vibronic-coupling approach*, chapter 7, pages 323–367. World Scientific Publ Co Pte Ltd, 2004.

[34] R. J. Bartlett and I. Shavitt, *Many-Body Methods in Chemistry and Physics: MBPT and Coupled-Cluster Theory*, Cambridge Molecular Science. Cambridge University Press, 1-532, 2009, ISBN: 978-0-511-59683-4.

[35] K. Sneskov and O. Christiansen, Excited state coupled cluster methods, WIREs: Comput. Mol. Sci. **2**, 566 (2012).

[36] R. J. Bartlett, Coupled-cluster theory and its equation-of-motion extensions, WIREs: Comput. Mol. Sci. **2**, 126 (2012).

[37] J. Almlöf and P. R. Taylor, General contraction of Gaussian basis sets. I. Atomic natural orbitals for first- and second-row atoms, J. Chem. Phys. **86**, 4070 (1987).

[38] J. Almlöf, T. Helgaker, and P. R. Taylor, Gaussian basis sets for high-quality ab initio calculations, J. Phys. Chem. **92**, 3029 (1988).

[39] J. F. Stanton and J. Gauss, A simple scheme for the direct calculation of ionization potentials with coupled-cluster theory that exploits established excitation energy methods, J. Chem. Phys.

111, 8785 (1999).

[40] T. Ichino, J. Gauss, and J. F. Stanton, Quasidiabatic states described by coupled-cluster theory, J. Chem. Phys. **130**, 174105 (2009).

[41] D. Woon and T. H. Dunning, Jr., Gaussian basis sets for use in correlated molecular calculations. V. Core-valence basis sets for boron through neon, J. Chem. Phys. **103**, 4572 (1995).

[42] K. A. Peterson and T. H. Dunning, Jr., Accurate correlation consistent basis sets for molecular core-valence correlation effects. the second row atoms Al-Ar, and the first row atoms B-Ne revisited, J. Chem. Phys. **117**, 10548 (2002).

[43] H. Müller, H. Köppel, L. S. Cederbaum, T. Schmelz, G. Chambaud, and P. Rosmus, Vibronic coupling effects in the ozone cation, Chem. Phys. Lett. **197**, 599 (1992).

[44] K. Sharma, O. A. Vasilyev, T. A. Miller, and J. F. Stanton, Molecules with spin and vibronic coupling effects: A computational perspective, in *Journal of Physics: Conference Series*, volume 2769, page 012002. IOP Publishing, 2024.

[45] J.F. Stanton, J. Gauss, M.E. Harding, and P.G. Szalay, CFOUR, with contributions from A.A. Auer, R.J. Bartlett, U. Benedikt, C. Berger, D.E. Bernholdt, Y.J. Bomble, L. Cheng, O. Christiansen, M. Heckert, O. Heun, C. Huber, T.-C. Jagau, D. Jonsson, J. Jusélius, K. Klein, W.J. Lauderdale, F. Lipparini, D.A. Matthews, T. Metzroth, L.A. Mück, D.P. O'Neill, D.R. Price, E. Prochnow, C. Puzzarini, K. Ruud, F. Schiffmann, W. Schwalbach, C. Simmons, S. Stopkowicz, A. Tajti, J. Vázquez, F. Wang, J.D. Watts; and the integral packages MOLECULE (J. Almlöf and P.R. Taylor), PROPS (P.R. Taylor), ABACUS (T. Helgaker, H.J.Aa. Jensen, P. Jørgensen, and J. Olsen), and ECP routines by A.V. Mitin and C. van Wüllen. For the current version, see http://www.cfour.de.

[46] D. A. Matthews, L. Cheng, M. E. Harding, F. Lipparini, S. Stopkowicz, T.-C. Jagau, P. G. Szalay, J. Gauss, and J. F. Stanton, Coupled-cluster techniques for computational chemistry: The CFOUR program package, J. Chem. Phys. **152**, 214108 (2020).

[47] R. Tarron and S. Carter, Ab initio study of vibronic coupling in the ozone radical cation, Chem. Phys. Lett. **511**, 201 (2011).

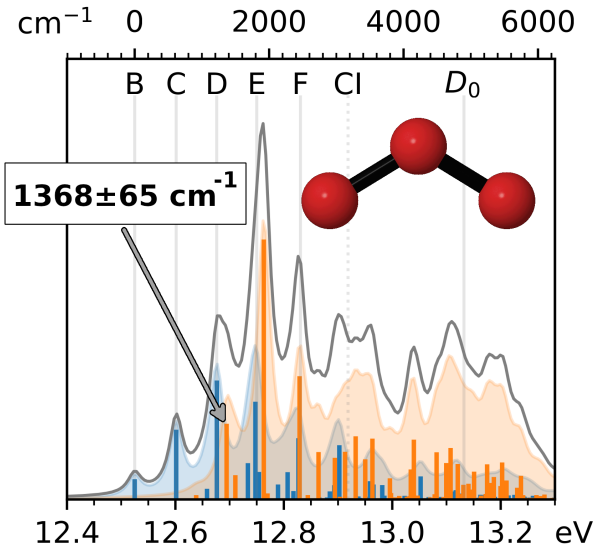

FIG. 10: TOC

Vibronic Coupling Effects in the Photoelectron Spectrum of Ozone: A Coupled-Cluster Approach: Supporting Information

Paweł Wójcik[a], Hanna Reisler[a], Péter G. Szalay[b], Anna I. Krylov[a,†], John F. Stanton[b,c,*]

[a] Department of Chemistry, University of Southern California, Los Angeles, California 90089, USA

[b] Laboratory of Theoretical Chemistry, Institute of Chemistry, ELTE

Eötvös Loránd University, Pázmány Péter stny. 1/A, Budapest, Hungary

[c] Quantum Theory Project, Departments of Chemistry and

Physics, University of Florida, Gainesville, FL, USA 32611

† krylov@usc.edu; * jfstanton137@gmail.com

(Dated: October 31, 2024)

S1. Parameters for the KDC Hamiltonian

Below is an input for the XSIM program, which contains all parameters used to define the KDC Hamiltonian.

```
Units
1
Dataset
1
States
2
Modes
3
Basis Functions
50 50 50
Lanczos
6000
Transition Moment
1. 1.35 ! Muller, Koppel, Cederbaum, et al. Chem. Phys. Lett. 197, 599 (1992)
Vertical Energies, cm-1
1 103456.7 ! EOMIP-CCSDT/pCVnZ/CBS n=5,6 + dQ/pwCVTZ + relativistic/CCSD/pwCVTZ
2 104449.7 ! EOMIP-CCSDT/pCVnZ/CBS n=5,6 + dQ/pwCVTZ + relativistic/CCSD/pwCVTZ
0 0 0 0 0 0 0 0 0 0 0 0
Harmonic Frequencies, cm-1 ! CCSDT/ANO1 for the neutral state
1 724.19
2 1168.58
3 1128.50
0 0 0 0 0 0 0 0 0 0 0 0
```

```
Linear, cm-1 ! Everything below: EOM-CCSDT/ANO1
1 1 2     1178.18
1 1 1     1261.02
2 2 2     -781.75
2 2 1    -1303.82
1 2 3     1393.82
0 0 0 0 0 0 0 0 0 0 0 0
Quadratic, cm-1
1 1 2 2      802.90
1 1 1 2     -185.50
1 1 1 1      779.81
2 2 2 2     1276.61
2 2 1 2       23.56
2 2 1 1      369.33
0 0 0 0 0 0 0 0 0 0 0 0
Cubic, cm-1
1 1 2 2 2     -202.85
1 1 1 2 2       74.39
1 1 1 1 2      -62.49
1 1 1 1 1       90.19
2 2 2 2 2     -282.04
2 2 1 2 2       75.56
2 2 1 1 2       -0.49
2 2 1 1 1       71.32
0 0 0 0 0 0 0 0 0 0 0 0
Quartic, cm-1
1 1 2 2 2 2       34.17
1 1 1 2 2 2      -26.65
1 1 1 1 2 2        3.16
1 1 1 1 1 2      -12.25
1 1 1 1 1 1        3.92
2 2 2 2 2 2       41.58
2 2 1 2 2 2      -35.55
2 2 1 1 2 2       -7.14
2 2 1 1 1 2       -6.88
2 2 1 1 1 1       11.34
0 0 0 0 0 0 0 0 0 0 0 0
```

S2. Relevant Cartesian Coordinates

The CCSDT/ANO1 geometry of neutral ozone (Å) (The nuclear repulsion energy: 68.994611948499568 a.u.)

```
Enuc=68.994612
O      0.0000    0.0000    0.4431
O      0.0000   -1.0817   -0.2215
O      0.0000    1.0817   -0.2215
```

The KDC Hamiltonian parameterization corresponds to this point.

S3. PES of the Ozone Cation

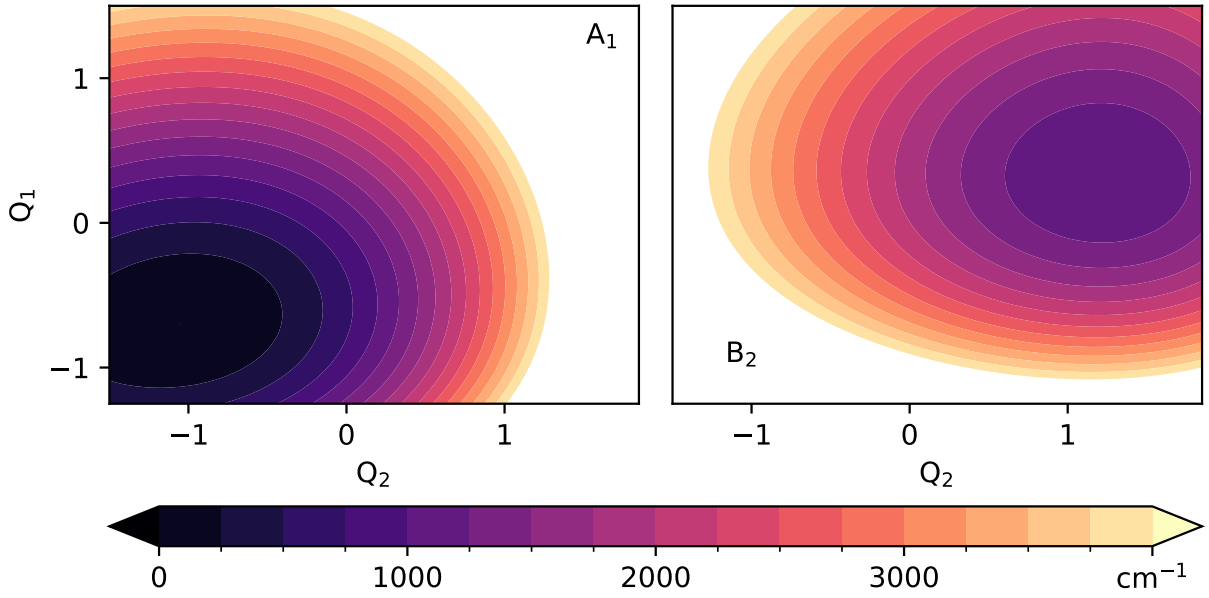

FIG. S1: Contour maps of the two diabatic PESs of the ozone cation (see Fig. 4 in the main text). Q_1 and Q_2 are two symmetric normal coordinates.